Immittance-Based Stability and Instability Participation Analysis for DC Microgrids

Bangbang He, *Member, IEEE*, Wu Chen, *Senior Member, IEEE*, Jianzhong Xu, *Senior Member, IEEE*, Han Mu, *Student Member, IEEE*, and Chengyong Zhao, *Senior Member, IEEE*

***Abstract*—The existing immittance-based stability analysis approaches for dc microgrids rarely account for the line network, and they are always troubled by the non-minimum phase issues. In this article, we introduce a novel method for stability analysis based on the determinant of the constructed immittance matrix. Since the determinant's right-half-plane poles are explicitly proven absent, it is only necessary to ascertain the net number of times that the phase trajectory crosses the $\pm 180^\circ$ line in system stability analysis. Subsequently, based on the immittance matrix decomposition and sensitivity calculation, a participation analysis method is further presented to identify the critical converter that dominates system instability. Finally, the simulation case of a 750 V 30 kW dc microgrid and the experiment case of a 24 V 180 W dc microgrid are established to validate these methods.**

***Index Terms*—DC microgrids, immittance, participation analysis, right-half-plane (RHP) pole, stability.**

I. Introduction

In response to global warming and its associated suite of severe environmental issues, low-carbon transition has become a global consensus. Vigorously developing renewable energy is one of the important measures to achieve low-carbon transformation of energy sector. DC microgrids can efficiently and friendly integrate renewable energy sources, such as photovoltaics and wind power, as well as dc loads like electric vehicles and data centers, which has been widely studied and applied [1], [2], [3]. Furthermore, dc microgrids have facilitated the transition from traditional centralized power generation to a distributed architecture, yielding the significant economic benefits [4]. However, due to the complicated interaction between numerous converters and passive networks, the small-signal stability remains a major concern for dc microgrids [5], [6].

At present, the stability analysis approach based on immittance (i.e., impedance and admittance) has become widely popular because of its clear physical meaning and measurability [7], [8], [9]. Generally, the immittances of all converters are used to construct a transfer function expression related to system stability. Then, whether the system characteristic roots are located in the right-half-plane (RHP) can be judged by the frequency-domain trajectory. Over the past half-century, many immittance-based stability criteria have been reported, such as the forbidden region criteria represented by the Middlebrook criterion [10], [11], impedance-ratio criterion [12], impedance-sum criterion [13], admittance-sum criterion [14], and global admittance criterion [15]. In [16], the existing five stability criteria are studied and compared in the interconnected converter systems. It is found that although they are equivalent in reflecting the system characteristic roots, they may all suffer from the non-minimum phase issue and zero-pole cancellation risk. In order to avoid these problems, the stability criterion without RHP poles was proposed in [17] and [18]. However, the criterion is only applicable to the highly centralized dc microgrid with multiple paralleled converters, where the line network is neglected.

According to the research conclusion of [9], in some cases, the line impedance may be beneficial to the stability of a dc microgrid, and ignoring the line network could lead to a misjudgment of system stability. To overcome this issue, Hu et al. [19] addressed the stability of the meshed dc distribution power system (DPS) with four nodes, and proposed a stability criterion based on the inverse impedance matrix. However, the method includes the complex inverse calculation of a fourth-order impedance matrix and 16 transfer functions should be assessed. Li et al. [20] investigated the stability of dc DPS with multiple nodes and complex network, and proposed two stability criteria based on admittance matrix sum and equivalent loop gain, respectively. However, these two methods not only face the RHP pole problem, but also include the complicated eigenvalue calculation of a high-order transfer function matrix. In order to simplify the analysis and calculation, He et al. [9] proposed a bus node impedance criterion, i.e., the system stability can be assessed by any bus node impedance, which is applicable to dc DPSs with and without a line network. However, this method still suffers from the non-minimum phase issue and relies on the detailed mathematical modeling.

Received 18 September 2024; revised 22 December 2024; accepted 2 February 2025. Date of publication 5 February 2025; date of current version 20 March 2025. This work was supported in part by the Beijing Natural Science Foundation under Grant 3254048 and Grant 3222059 and in part by the China Postdoctoral Science Foundation under Grant 2024M760901. Recommended for publication by Associate Editor M. Molinas. *(Corresponding author: Wu Chen.)*

Bangbang He, Jianzhong Xu, and Chengyong Zhao are with the School of Electrical and Electronic Engineering, North China Electric Power University (NCEPU), Beijing 102206, China (e-mail: hbb@ncepu.edu.cn; xujianzhong@ncepu.edu.cn; chengyongzhao@ncepu.edu.cn).

Wu Chen is with the Center for Advanced Power Conversion Technology and Equipment, School of Electrical Engineering, Southeast University, Nanjing 210096, China (e-mail: chenwu@seu.edu.cn).

Han Mu is with the Department of Electrical Engineering, Eindhoven University of Technology, 5612 AP Eindhoven, The Netherlands (e-mail: h.mu@tue.nl).

Color versions of one or more figures in this article are available at https://doi.org/10.1109/TPEL.2025.3538898.

Digital Object Identifier 10.1109/TPEL.2025.3538898

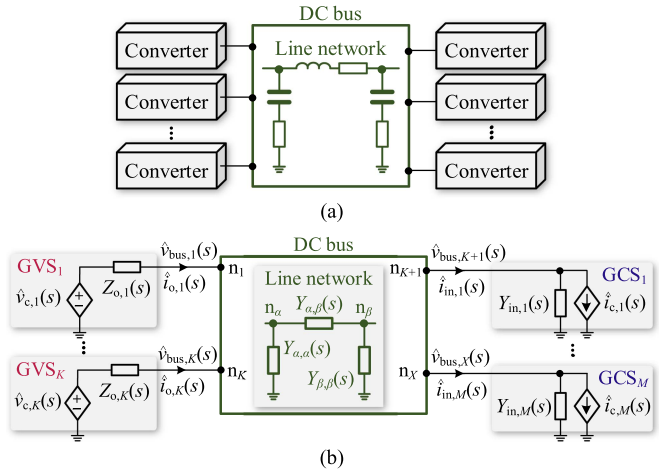

Fig. 1. Typical structure and small-signal equivalent model of the dc microgrid. (a) System structure. (b) Small-signal equivalent model.

Besides, when dc microgrid is unstable, it is necessary to analyze the participation of each converter in system oscillation and identify the critical instability sources, which can further facilitate design-oriented stability improvement. The traditional participation analysis is based on the eigenvalues of the state-space matrix [21], which requires the complete parameters of the entire system. Recently, several frequency-domain participation analysis approaches have been reported [22], [23], [24], [25], [26], most of them are based on the return-ratio matrix of ac electronic power systems. The frequency-domain analysis method is more suitable for the larger scale power systems with dc microgrids with unknown parameters or grey-box models, and the parameter sensitivity can also be further calculated according to the chain rule [24], [25]. However, the existing methods cannot be directly applied to dc microgrid due to the possible existence of RHP poles in the corresponding stability criteria.

In order to address the aforementioned challenges, this article aims to propose a novel stability analysis method for dc microgrid considering the line network, wherein the RHP pole issue can be completely avoided. Based on this, the participation analysis method will be further presented to identify the critical converter responsible for system instability. Finally, case studies, simulations, and experiments will validate these methods.

II. System Modeling and Stability Analysis

A. System Description and Small-Signal Modeling

Fig. 1(a) shows a typical dc microgrid, where each converter is connected to a different dc bus node, and the interconnection among various dc bus nodes constitutes the line network. All converters can be divided into the following two categories [27].

1) The converter that controls dc bus voltage is classified as a generalized voltage source (GVS), which can be represented by the Thevenin model in small-signal analysis.
2) The converter that controls dc bus current is classified as a generalized current source (GCS), which can be represented by the Norton model in small-signal analysis.

Meanwhile, the line network is modeled by the node admittance matrix. Then, we can build the small-signal equivalent circuit model of dc microgrid, as shown in Fig. 1(b). In order to facilitate analysis, some basic assumptions are given as follows.

1) The entire system contains K GVSs, M GCSs and X nodes, where $X = K + M$.
2) All GVSs are connected to the first K nodes and marked as GVS_1, ⋯, GVS_j, ⋯, and GVS_K in sequence, while all GCSs are connected to the remaining nodes and marked as GCS_1, ⋯, GCS_l, ⋯, and GCS_M in sequence.
3) $v_{c,j}(s)$, $Z_{o,j}(s)$, and $i_{o,j}(s)$ are the controlled voltage source, output impedance, and output current of GVS_j, respectively. $i_{\mathrm{c},l}(s)$, $Y_{\mathrm{in},l}(s)$, and $i_{\mathrm{in},l}(s)$ denote the controlled current source, input admittance, and input current of GCS_l, respectively.
4) $v_{\mathrm{bus},\alpha}$ is the voltage of dc bus node n_α, where $\alpha = 1, 2, \cdots, X$.
5) $Y_{\alpha,\alpha}(s)$ is the self-admittance of n_α, and $Y_{\alpha,\beta}(s)$ is the mutual admittance between nodes n_α and n_β.
6) The symbol with "^" represents the small-signal form of the corresponding variable.

According to the circuit theory and network analysis method, the node voltage equation of the system shown in Fig. 1 can be derived as

$$\hat{\boldsymbol{v}}_{\mathrm{bus}}(s) = \boldsymbol{T}_{\mathrm{m}}^{-1}(s)\hat{\boldsymbol{h}}(s) \tag{1}$$

where

$$\hat{\boldsymbol{v}}_{\mathrm{bus}}(s) = \left[\hat{v}_{\mathrm{bus},1}(s), \cdots, \hat{v}_{\mathrm{bus},K}(s), \hat{v}_{\mathrm{bus},K+1}(s), \cdots, \hat{v}_{\mathrm{bus},X}(s)\right]^T \tag{2}$$

$$\boldsymbol{T}_m(s) = \boldsymbol{Y}_{\mathrm{in}}(s) + \boldsymbol{Z}_o(s)\boldsymbol{Y}_{\mathrm{net}}(s) \tag{3}$$

$$\hat{\boldsymbol{h}}(s) = \left[\hat{v}_{c,1}(s), \cdots, \hat{v}_{c,K}(s), \hat{i}_{c,1}(s), \cdots, \hat{i}_{c,M}(s)\right]^T. \tag{4}$$

In (3), $\boldsymbol{T}_m(s)$ is the constructed immittance matrix; $\boldsymbol{Y}_{\mathrm{in}}(s)$ and $\boldsymbol{Z}_o(s)$ are Xth-order diagonal matrices composed of the input admittances of all GCSs and the output impedances of all GVSs, respectively; $\boldsymbol{Y}_{\mathrm{net}}(s)$ is the nodal admittance matrix of the line network. The expressions of $\boldsymbol{Y}_{\mathrm{in}}(s)$, $\boldsymbol{Z}_o(s)$, and $\boldsymbol{Y}_{\mathrm{net}}(s)$ are given as

$$\boldsymbol{Y}_{\mathrm{in}}(s) = \mathrm{diag}\ \left[1, \cdots, 1, -Y_{\mathrm{in},1}(s), \cdots, -Y_{\mathrm{in},M}(s)\right] \tag{5}$$

$$\boldsymbol{Z}_{\mathrm{o}}(s) = \mathrm{diag}\ \left[Z_{o,1}(s), \cdots, Z_{o,K}(s), -1, \cdots, -1\right] \tag{6}$$

$$\boldsymbol{Y}_{\mathrm{net}}(s) = \begin{bmatrix} \sum_{\alpha=1}^{X} Y_{\alpha,1}(s) & -Y_{1,2}(s) & \cdots & -Y_{1,X}(s) \\ -Y_{2,1}(s) & \sum_{\alpha=1}^{X} Y_{\alpha,2}(s) & \cdots & -Y_{2,X}(s) \\ \vdots & \vdots & & \vdots \\ -Y_{X,1}(s) & -Y_{X,2}(s) & \cdots & \sum_{\alpha=1}^{X} Y_{\alpha,X}(s) \end{bmatrix}. \tag{7}$$

B. System Stability Analysis

The stability of dc microgrid depicted in Fig. 1 refers to the voltage stability of each dc bus node. According to the control theory, the dc microgrid is stable *if and only if* the inverse of $\boldsymbol{T}_{\mathrm{m}}(s)$ has no RHP poles. The inverse of $\boldsymbol{T}_m(s)$ can be

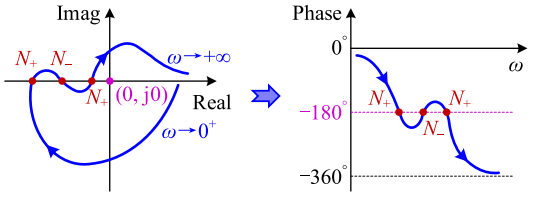

Fig. 2. Equivalent phase crossing in Nyquist contour and Bode plot.

expressed as (8), where adj[] and det[] are used to compute the adjoint and determinant of a matrix, respectively,

$$\boldsymbol{T}_m^{-1}(s) = \frac{\text{adj}\left[\boldsymbol{T}_m(s)\right]}{\det\left[\boldsymbol{T}_m(s)\right]} = \frac{\text{adj}\left[\boldsymbol{Y}_{\text{in}}(s) + \boldsymbol{Z}_o(s)\boldsymbol{Y}_{\text{net}}(s)\right]}{\det\left[\boldsymbol{Y}_{\text{in}}(s) + \boldsymbol{Z}_o(s)\boldsymbol{Y}_{\text{net}}(s)\right]}. \tag{8}$$

The stability analysis for a complicated power system typically begins with the assumption that all converters are stable in their standalone operation conditions. Then, both $Z_{o,j}(s)$ and $Y_{\text{in},l}(s)$ do not contain any RHP pole. In addition, since the line network is passive, $\boldsymbol{Y}_{\text{net}}(s)$ also has no RHP zeros or poles. Given that the matrix's adjoint and determinant operations only involve the addition and multiplication, neither adj[$\boldsymbol{T}_m(s)$] nor det[$\boldsymbol{T}_m(s)$] contains RHP poles.

Based on the aforementioned analysis, when det[$\boldsymbol{T}_m(s)$] has no RHP zeros, the dc microgrid is stable, and vice versa. According to the Cauchy's argument principle, whether det[$\boldsymbol{T}_m(s)$] has RHP zeros is equivalent to whether its Nyquist contour encircles the origin clockwise. As illustrated in Fig. 2, the number of times that the Nyquist contour of det[$\boldsymbol{T}_m(s)$] clockwise encircles the origin can be calculated as $2(N_+–N_–)$ in the Bode plot, where N_+ and $N_–$ denote the number of times that the phase trajectory crosses the $\pm 180°$ line from above to below and from below to above, respectively. Note that if the phase trajectory starts or ends at the $\pm 180°$ line from the top down, N_+ is counted as 0.5. Conversely, if the phase trajectory starts or ends at the $\pm 180°$ line from the bottom up, $N_–$ is counted as 0.5.

In summary, the stability criterion based on the determinant of the immittance matrix can be described as follows. It can be seen that this criterion only requires the phase information to assess the system stability, which is easier and more feasible.

Criterion: The dc microgrid depicted in Fig. 1 is stable *if and only if* the net number of times that the phase trajectory of det[$\boldsymbol{T}_m(s)$] crosses the line at $\pm 180°$, i.e., $N_+–N_–$, is zero.

III. Instability Participation Analysis

Based on the proposed stability criterion, this section will further propose an instability participation analysis method for dc microgrid when it operates unstably.

A. Matrix Decomposition of $\boldsymbol{T}_m(s)$

Assume that the eigenvalues of the immittance matrix $\boldsymbol{T}_m(s)$ are $\lambda_1(s), \cdots, \lambda_\alpha(s), \cdots$, and $\lambda_X(s)$, respectively. Then, there is

$$\det\left[\boldsymbol{T}_m(s)\right] = \lambda_1(s)\cdots\lambda_\alpha(s)\cdots\lambda_X(s). \tag{9}$$

Since $\boldsymbol{T}_m(s)$ always has no RHP poles, there also must be no RHP poles in each of its eigenvalues. Since the system stability depends on the absence of RHP zeros in det[$\boldsymbol{T}_m(s)$], the presence of RHP poles in any eigenvalue of det[$\boldsymbol{T}_m(s)$] can also indicate the instability of dc microgrid.

According to the matrix decomposition theory, there is

$$\boldsymbol{T}_m(s) = \boldsymbol{\Phi}(s)\boldsymbol{\Lambda}(s)\boldsymbol{\Psi}(s) \tag{10}$$

where $\boldsymbol{\Phi}(s)$ is the right eigenvector matrix of $\boldsymbol{T}_m(s)$, $\boldsymbol{\Lambda}(s)$ is the diagonal matrix of eigenvalues, and $\boldsymbol{\Psi}(s)$ is the left eigenvector matrix, with their specific forms given as

$$\boldsymbol{\Phi}(s) = \left[\boldsymbol{\varphi}_1(s), \cdots, \boldsymbol{\varphi}_\alpha(s), \cdots, \boldsymbol{\varphi}_X(s)\right] \tag{11}$$

$$\boldsymbol{\Lambda}(s) = \text{diag}\left[\lambda_1(s), \cdots, \lambda_\alpha(s), \cdots, \lambda_X(s)\right] \tag{12}$$

$$\boldsymbol{\Psi}(s) = \left[\boldsymbol{\psi}_1^T(s), \cdots, \boldsymbol{\psi}_\alpha^T(s), \cdots, \boldsymbol{\psi}_X^T(s)\right]^T \tag{13}$$

where $\boldsymbol{\varphi}_\alpha(s)$ and $\boldsymbol{\psi}_\alpha^T(s)$ are the right and left column eigenvectors of $\lambda_\alpha(s)$, respectively, detailed as

$$\boldsymbol{\varphi}_\alpha(s) = \left[\varphi_{1,\alpha}(s), \cdots, \varphi_{\alpha,\alpha}(s), \cdots, \varphi_{X,\alpha}(s)\right]^T \tag{14}$$

$$\boldsymbol{\psi}_\alpha(s) = \left[\psi_{\alpha,1}(s), \cdots, \psi_{\alpha,\alpha}(s), \cdots, \psi_{\alpha,X}(s)\right]. \tag{15}$$

From (10)–(15), the following equations can be obtained, where $\boldsymbol{E}$ is the identity matrix

$$\boldsymbol{\Phi}(s)\boldsymbol{\Psi}(s) = \boldsymbol{E} \text{ and } \boldsymbol{\psi}_\alpha(\text{s})\boldsymbol{\varphi}_\alpha(\text{s}) = 1 \tag{16}$$

$$\boldsymbol{T}_m(s)\boldsymbol{\varphi}_\alpha(s) = \lambda_\alpha(s)\boldsymbol{\varphi}_\alpha(s) \tag{17}$$

$$\boldsymbol{\psi}_\alpha(s)\boldsymbol{T}_m(s) = \lambda_\alpha(s)\boldsymbol{\psi}_\alpha(s) \tag{18}$$

$$\lambda_\alpha(s) = \boldsymbol{\psi}_\alpha(s)\boldsymbol{T}_m(s)\boldsymbol{\varphi}_\alpha(s). \tag{19}$$

B. Instability Participation Analysis Based on $\boldsymbol{T}_m(s)$

Substituting (10) and (16) into (1), yields that

$$\boldsymbol{\Psi}(s)\hat{\boldsymbol{v}}_{\text{bus}}(s) = \boldsymbol{\Lambda}^{-1}(s)\boldsymbol{\Psi}(s)\hat{\boldsymbol{h}}(s). \tag{20}$$

According to [28], we can define (21) and (22) as the modal bus node voltage and the modal input disturbance, respectively,

$$\hat{\boldsymbol{V}}_n(s) = \boldsymbol{\Psi}(s)\hat{\boldsymbol{v}}_{\text{bus}}(s) \tag{21}$$

$$\hat{\boldsymbol{H}}(s) = \boldsymbol{\Psi}(s)\hat{\boldsymbol{h}}(s). \tag{22}$$

Then, (20) can be further simplified to

$$\hat{\boldsymbol{V}}_{\text{n}}(s) = \boldsymbol{\Lambda}^{-1}(s)\hat{\mathbf{H}}(s) \quad \text{or}$$

$$\begin{bmatrix} \hat{V}_{n,1}(s) \\ \vdots \\ \hat{V}_{n,\alpha}(s) \\ \vdots \\ \hat{V}_{n,X}(s) \end{bmatrix} = \begin{bmatrix} \lambda_1^{-1}(s) & & & & \\ & \ddots & & & \\ & & \lambda_\alpha^{-1}(s) & & \\ & & & \ddots & \\ & & & & \lambda_X^{-1}(s) \end{bmatrix} \begin{bmatrix} \hat{H}_1(s) \\ \vdots \\ \hat{H}_\alpha(s) \\ \vdots \\ \hat{H}_X(s) \end{bmatrix}. \tag{23}$$

From (23), it can be seen that each modal bus node voltage is decoupled from the others. When the magnitude of $\lambda_\alpha(s)$ is minimum (i.e., close to zero), a smaller modal input disturbance $\hat{H}_\alpha(s)$ will lead to a significant modal bus node voltage $\hat{V}_{n,\alpha}(s)$. Meanwhile, other modal bus node voltages will not be affected,

as there is no coupling between them and $\hat{H}_\alpha(s)$. Thus, at the oscillation frequency $f_{\rm osc}$, the eigenvalue $\lambda_\alpha(s)$ with the smallest amplitude can be considered critical.

Inspired by [26], the participation factors $p_{\alpha,j}(s)$ and $p_{\alpha,l}(s)$ are derived as (24) and (25), respectively, Here, $\boldsymbol{y}_{\rm net,j}(s)$ is a vector containing the elements of the jth row of $\boldsymbol{Y}_{\rm net}(s)$

$$\begin{aligned}
p_{\alpha,j}(s) &= \frac{\partial\lambda_\alpha(s)}{\partial Z_{{\rm o},j}(s)} \overset{(19)}{=} \frac{\partial\left[\boldsymbol{\psi}_\alpha(s)\boldsymbol{T}_m(s)\boldsymbol{\varphi}_\alpha(s)\right]}{\partial Z_{{\rm o},j}(s)} \\
&= \frac{\partial\boldsymbol{\psi}_\alpha(s)}{\partial Z_{{\rm o},j}(s)}\boldsymbol{T}_m(s)\boldsymbol{\varphi}_\alpha(s) + \boldsymbol{\psi}_\alpha(s)\frac{\partial\boldsymbol{T}_{\rm m}(s)}{\partial Z_{o,j}(s)}\boldsymbol{\varphi}_\alpha(s) \\
&\quad + \boldsymbol{\psi}_\alpha(s)\boldsymbol{T}_m(s)\frac{\partial\boldsymbol{\varphi}_\alpha(s)}{\partial Z_{{\rm o},j}(s)} \\
&\overset{(17)\text{and}(18)}{=} \lambda_\alpha(s)\frac{\partial\left[\boldsymbol{\psi}_\alpha(s)\boldsymbol{\varphi}_\alpha(s)\right]}{\partial Z_{o,j}(s)} + \boldsymbol{\psi}_\alpha(s)\frac{\partial\boldsymbol{T}_{\rm m}(s)}{\partial Z_{o,j}(s)}\boldsymbol{\varphi}_\alpha(s) \\
&\overset{(3),(5),\text{and}(16)}{=} \boldsymbol{\psi}_\alpha(s)\left[\frac{\partial\boldsymbol{Z}_o(s)}{\partial Z_{o,j}(s)}\boldsymbol{Y}_{\rm net}(s)\right]\boldsymbol{\varphi}_\alpha(s) \\
&\overset{(6)\text{and}(7)}{=} \psi_{\alpha,j}(s)\boldsymbol{y}_{{\rm net},j}(s)\boldsymbol{\varphi}_\alpha(s)
\end{aligned} \tag{24}$$

$$\begin{aligned}
p_{\alpha,l}(s) &= \frac{\partial\lambda_\alpha(s)}{\partial Y_{{\rm in},l}(s)} \overset{(19)}{=} \frac{\partial\left[\boldsymbol{\psi}_\alpha(s)\boldsymbol{T}_m(s)\boldsymbol{\varphi}_\alpha(s)\right]}{\partial Y_{{\rm in},l}(s)} \\
&= \frac{\partial\boldsymbol{\psi}_\alpha(s)}{\partial Y_{{\rm in},l}(s)}\boldsymbol{T}_m(s)\boldsymbol{\varphi}_\alpha(s) + \boldsymbol{\psi}_\alpha(s)\frac{\partial\boldsymbol{T}_m(s)}{\partial Y_{{\rm in},l}(s)}\boldsymbol{\varphi}_\alpha(s) \\
&\quad + \boldsymbol{\psi}_\alpha(s)\boldsymbol{T}_m(s)\frac{\partial\boldsymbol{\varphi}_\alpha(s)}{\partial Y_{{\rm in},l}(s)} \\
&\overset{(17)\text{and}(18)}{=} \lambda_\alpha(s)\frac{\partial\left[\boldsymbol{\psi}_\alpha(s)\boldsymbol{\varphi}_\alpha(s)\right]}{\partial Y_{{\rm in},l}(s)} + \boldsymbol{\psi}_\alpha(s)\frac{\partial\boldsymbol{T}_m(s)}{\partial Y_{{\rm in},l}(s)}\boldsymbol{\varphi}_\alpha(s) \\
&\overset{(3),(6),(7),\text{and}(16)}{=} \boldsymbol{\psi}_\alpha(s)\frac{\partial\boldsymbol{Y}_{\rm in}(s)}{\partial Y_{{\rm in},l}(s)}\boldsymbol{\varphi}_\alpha(s) \\
&\overset{(5)}{=} -\psi_{\alpha,K+l}(s)\varphi_{K+l,\alpha}(s).
\end{aligned} \tag{25}$$

Note that the divided participation factors are not completely consistent with the existing frequency-domain participation factors, which is caused by the different stability criteria. $p_{\alpha,j}(s)$ and $p_{\alpha,l}(s)$ represent the sensitivity of $\lambda_\alpha(s)$ to $Z_{o,j}(s)$ and $Y_{{\rm in},l}(s)$ in $\boldsymbol{T}_m(s)$, respectively. Therefore, the participation and sensitivity level of GVS$_j$ and GCS$_l$ to $\lambda_\alpha(s)$ can be reflected by the magnitude of $p_{\alpha,j}(s)$ and $p_{\alpha,l}(s)$, respectively. In other words, the larger $|p_{\alpha,j}(s)|$ and $|p_{\alpha,l}(s)|$ are, the more relevant GVS$_j$ and GCS$_l$ are to $\lambda_\alpha(s)$, respectively. In summary, the converter corresponding to the largest participation factor can be identified as the critical instability source.

IV. Case Studies and Experiments

To fully validate the correctness and effectiveness of the proposed methods, a 750 V 30 kW dc microgrid and its simulation are constructed in MATLAB/Simulink, and a 24 V 180 W dc microgrid and its prototype are established in the lab.

TABLE I
Main Parameters of the First Case System

Symbol	Value	Symbol	Value	Symbol	Value
u_{abc}(RMS)	220 V	$L_{n,1}$	100 μH	R_3	5 Ω
L_f	10 mH	$R_{Ln,1}$	0.1 Ω	$i_{o,3}$	50 A
R_f	0.5 Ω	$L_{n,2}$	100 μH	$k_{p,3}$	0.3
$C_{\rm dc}$	100 μF	$R_{Ln,2}$	0.1 Ω	$k_{i,3}$	300
k_{vi}	2000	$v_{\rm dc}$	200 V	$L_{{\rm f},4}$	100 μH
k_{ip}	50	L_2	1 mH	$R_{Lf,4}$	0.1 Ω
k_{ii}	200	$R_{L,2}$	0.1 Ω	$C_{f,4}$	100 μF
$L_{f,1}$	300 μH	C_2	500 μF	$R_{Cf,4}$	0.1 Ω
$R_{Lf,1}$	0.25 Ω	$R_{C,2}$	0.1 Ω	L_4	500 μH
$C_{f,1}$	100 μF	$i_{o,2}$	4 A	$R_{L,4}$	0.1 Ω
$R_{Cf,1}$	0.1 Ω	$k_{p,2}$	0.02	C_4	30 μF
L_1	500 μH	$k_{i,2}$	300	$R_{C,4}$	0.1 Ω
$R_{L,1}$	0.1 Ω	$L_{f,3}$	100 μH	R_4	10 Ω
C_1	100 μF	$R_{Lf,3}$	0.1 Ω	$v_{o,4}$	200 V
$R_{C,1}$	0.1 Ω	$C_{f,3}$	100 μF	$k_{p,4}$	0.5
R_1	11 Ω	L_3	500 μH	$k_{i,4}$	400
$v_{o,1}$	375 V	$R_{L,3}$	0.1 Ω	R	1500 Ω
$k_{p,1}$	0.2	C_3	100 μF	$L_{n,3}$	200 μH
$k_{i,1}$	300	$R_{C,3}$	0.1 Ω	$R_{Ln,3}$	0.15 Ω

A. Case Study of A 750 V 30 kW DC Microgrid

Fig. 3 shows the structure and topology of the 750 V 30 kW dc microgrid, which is composed of five converters and a resistive load. The main parameters of the system are listed in Table I, where the expressions of all controllers are $G_v(s) = k_{vp} + k_{vi}/s$, $\boldsymbol{G}_i(s) = [k_{\rm ip} + k_{ii}/s,\ 0;\ 0,\ k_{ip} + k_{ii}/s]$, $G_{v,1}(s) = k_{p,1} + k_{i,1}/s$, $G_{i,2}(s) = k_{p,2} + k_{i,2}/s$, $G_{i,3}(s) = k_{p,3} + k_{i,3}/s$, and $G_{v,4}(s) = k_{p,4} + k_{i,4}/s$. To assess the system stability under different operating conditions, two cases with different proportional coefficients of voltage outer loop in #1 converter are set: case I: $k_{vp} = 30$ and case II: $k_{vp} = 60$.

1) Stability Analysis: According to (5)–(7) and Fig. 3, there are

$$\boldsymbol{Y}_{\rm in}(s) = {\rm diag}\left[1,\ -Y_2(s),\ -Y_3(s) - Y_4(s) - 1/R,\ -Y_5(s)\right] \tag{26}$$

$$\boldsymbol{Z}_{\rm o}(s) = {\rm diag}\left[Z_1(s),\ -1,\ -1,\ -1\right] \tag{27}$$

$$\boldsymbol{Y}_{\rm net}(s) = \begin{bmatrix} Y_{1,2}(s) & -Y_{1,2}(s) & 0 & 0 \\ -Y_{1,2}(s) & Y_{1,2}(s)+Y_{2,3}(s) & -Y_{2,3}(s) & 0 \\ 0 & -Y_{2,3}(s) & Y_{2,3}(s)+Y_{3,4}(s) & -Y_{3,4}(s) \\ 0 & 0 & -Y_{3,4}(s) & Y_{3,4}(s) \end{bmatrix}. \tag{28}$$

By substituting (26)–(28) into (3), the pole-zero plots of the determinant det$[\boldsymbol{T}_m(s)]$ in two cases can be drawn, as shown in Fig. 4. It can be seen that there are no RHP zeros in det$[\boldsymbol{T}_m(s)]$ when the system operates in case I, while in case II, there is a pair of RHP zeros at 1330 Hz. Therefore, it can be inferred that the dc microgrid is stable in case I but unstable in case II with the oscillation frequency being approximately 1330 Hz. In fact, this stability conclusion can also be drawn from the Bode plots of det$[\boldsymbol{T}_{\rm m}(s)]$. As depicted in Fig. 5, in case I, there is N_+–N_- = 2–2 = 0, indicating that the net number of times

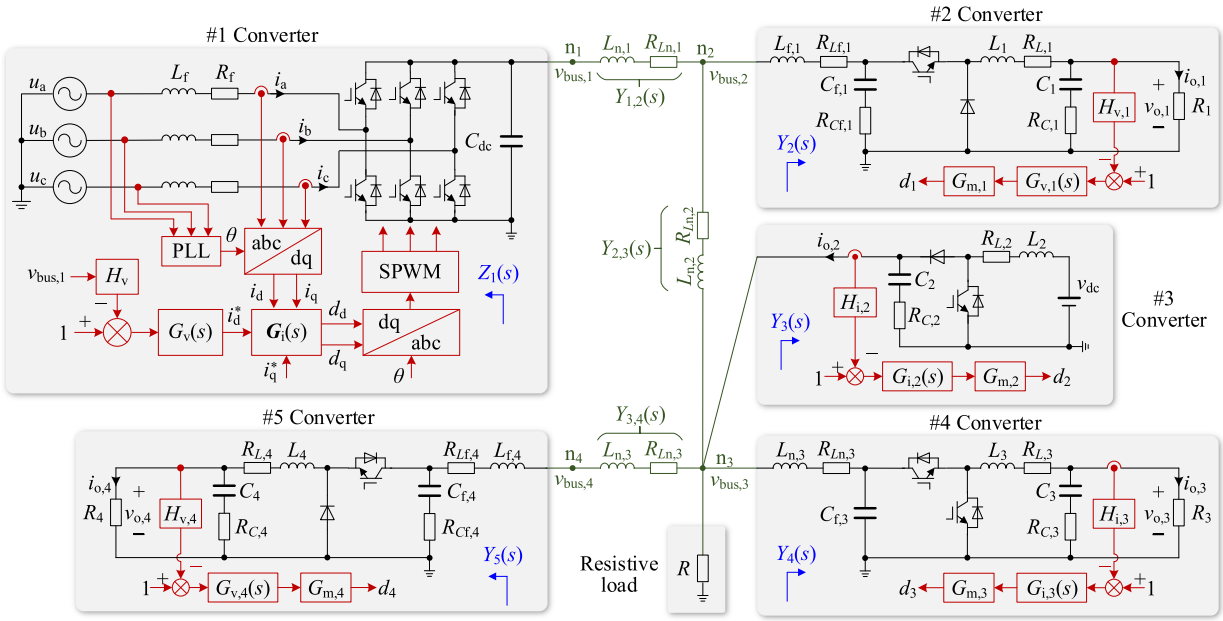

Fig. 3. Structure and topology of a 750 V 30 kW dc microgrid.

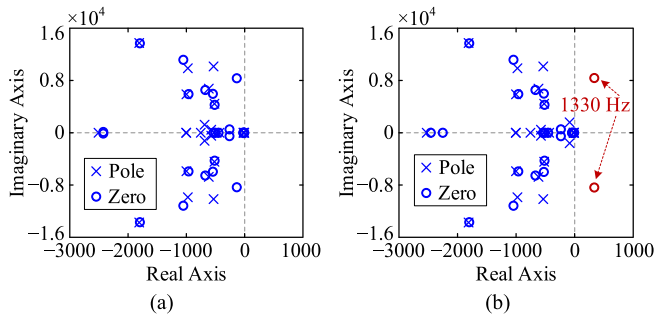

Fig. 4. Pole-zero plots of det[$\boldsymbol{T}_m(s)$] in two cases. (a) case I. (b) case II.

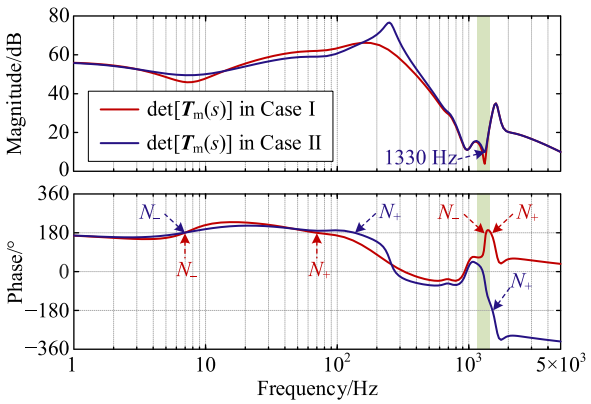

Fig. 5. Bode plots of det[$\boldsymbol{T}_m(s)$] in two cases.

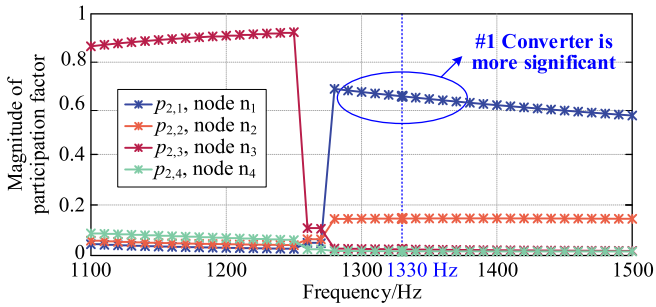

Fig. 6. Participation analysis of case II.

that the phase trajectory of det[$\boldsymbol{T}_m(s)$] crosses the $\pm 180°$ line is 0. In case II, there is $N_+ – N_- = 2 – 1 = 1$, indicating that the Nyquist contour of det[$\boldsymbol{T}_m(s)$] clockwise encircles the origin twice. Meanwhile, the instability frequency of case II can be predicted as 1330 Hz, where the magnitude of det[$\boldsymbol{T}_m(s)$] is locally minimum and the phase then rapidly drops by 180°.

2) Instability Participation Analysis: According to the above analysis, four eigenvalues of $\boldsymbol{T}_m(s)$ at 1065 Hz are further calculated as $\lambda_1 = -1.1616 + j3.4200$, $\lambda_2 = 0.0047 + j0.0865$, $\lambda_3 = -1.8864 – j4.6140$, and $\lambda_4 = -1.3277 – j1.4895$. Clearly, λ_2 has the smallest magnitude, thus it is the critical eigenvalue of case II. Then, the participation factors of λ_2, that is, $p_{2,1}$, $p_{2,2}$, $p_{2,3}$, and $p_{2,4}$, can be calculated and their magnitudes are plotted in Fig. 6. It is observed that around the predicted oscillation frequency, the participation factor of dc bus node n_1 is significantly higher than the others, indicating that #1 converter has the highest instability participation in case II. In other words, the system stability in case II is mainly sensitive to #1 converter.

3) Simulation Validations: As shown in Fig. 7(a) , all voltage and current waveforms are stable, indicating that the entire system operates stably in case I. However, when the system operates in case II, as shown in Fig. 7(b), there is a significant ac component in the voltage of each dc bus node, thus, the dc microgrid is unstable in this case. Fig. 8 shows the dynamic

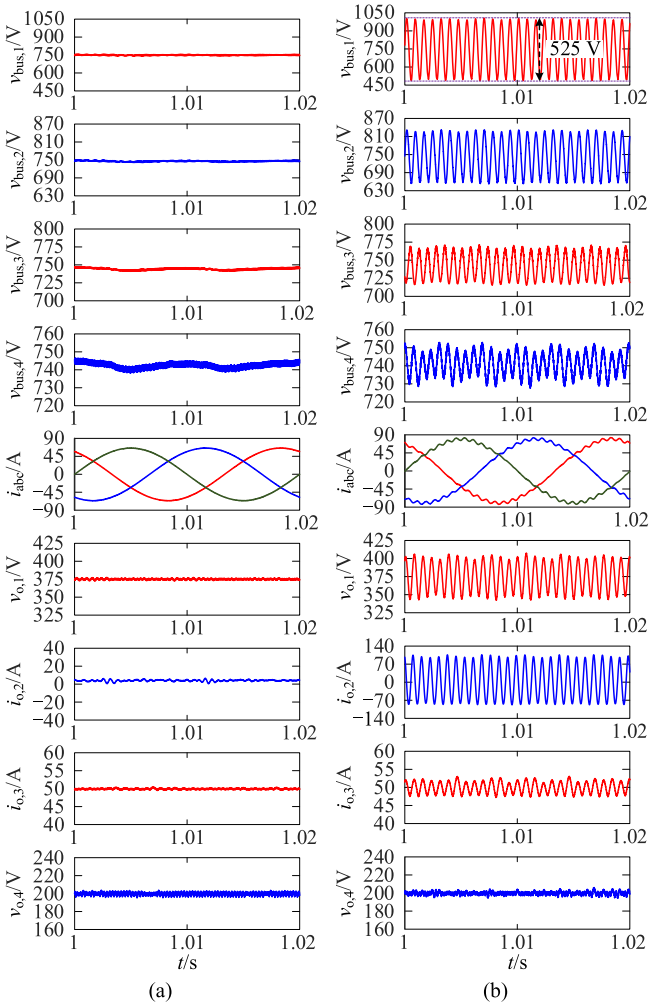

Fig. 7. Simulation waveforms in two cases. (a) case I. (b) case II.

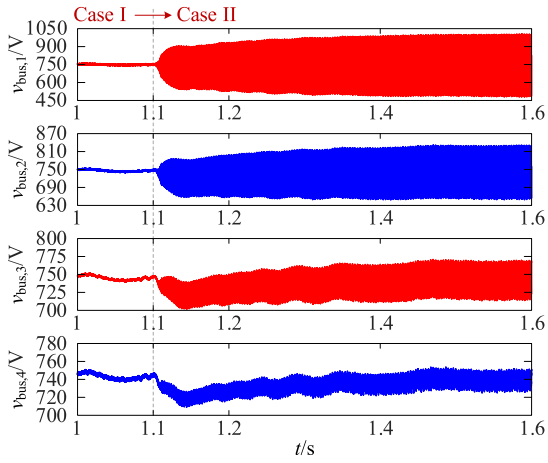

Fig. 8. Dynamic Simulation waveforms from case I to case II.

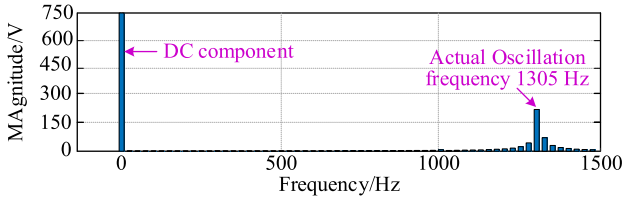

Fig. 9. FFT result of $v_{\text{bus},1}$ in case II.

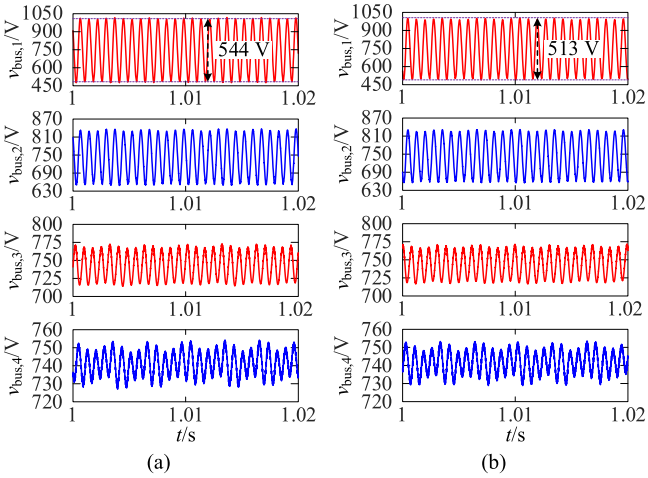

Fig. 10. Voltage waveforms of four dc bus nodes. (a) When $k_{p,1}$ is reduced by 50%. (b) When $k_{p,1}$ increases by 50%.

Simulation waveforms from case I to case II. Performing a fast Fourier transform (FFT) on $v_{\text{bus},1}$ of case II, the results are displayed in Fig. 9. It can be seen that the actual oscillation frequency is 1305 Hz, which is essentially consistent with the predicted instability frequency mentioned above.

Compared with the two cases, it can be found that when the proportional coefficient k_{vp} of the voltage outer loop of # 1 converter decreases by 50%, the system transitions from an unstable to a stable state. From Fig. 6, the amplitude of the participation factor of node n_2 is significantly smaller than that of node n_1. Therefore, if the proportional coefficient of the voltage loop of # 2 converter, that is, $k_{p,1}$, also changes by 50%, the system is still in an unstable state with the smaller oscillation amplitude change, as shown in Fig. 10. Therefore, #1 converter is confirmed to be the critical instability source of the dc microgrid in case II.

In summary, the simulation results validate the correctness of the proposed stability criterion and instability participation analysis methods.

B. Case Study of A 24 V 180 W DC Microgrid

The topology and experimental prototype of the 24 V 180 W dc microgrid are given in Fig. 11, where both #1 and #2 converters adopt the voltage droop control mode, while #3 and #4 converters provide the stable voltages $v_{o,3}$ and $v_{o,4}$ to load resistors R_3 and R_4, respectively. The main parameters of the system are given in Table II, where $G_{v,x}(s) = k_{vp,x} + k_{vi,x}/s\,(x = 1, 2, 3, 4)$ is the controller of #x converter. The switching frequency of each converter is 40 kHz. There are also two system cases: case III: $R_4 = 3\ \Omega$ and case IV: $R_4 = 1.5\ \Omega$.

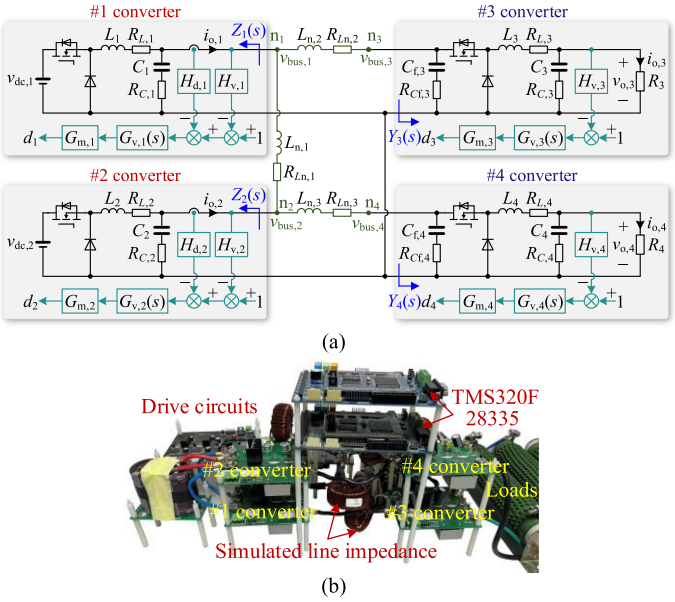

Fig. 11. 24 V 180 W dc Microgrid. (a) System topology. (b) Prototype.

TABLE II
MAIN PARAMETERS OF THE SECOND CASE SYSTEM

Symbol	Value	Symbol	Value	Symbol	Value
$v_{dc,1}$, $v_{dc,2}$	48 V	$L_{n,2}$	100 μH	$L_{n,3}$	200 μH
L_1, L_2	1 mH	$R_{Ln,2}$	0.05 Ω	$R_{Ln,3}$	0.05 Ω
$R_{L,1}$, $R_{L,2}$	0.12 Ω	$C_{f,3}$	100 μF	$C_{f,4}$	200 μF
C_1, C_2	90 μF	$R_{Cf,3}$	0.1 Ω	$R_{Cf,4}$	0.1 Ω
$R_{C,1}$, $R_{C,2}$	0.1 Ω	L_3	200 μH	L_4	500 μH
$H_{d,1}$, $H_{d,2}$	0.05/24	$R_{L,3}$	0.05 Ω	$R_{L,4}$	0.1 Ω
$k_{vp,1}$	0.13	C_3	39 μF	C_4	90 μF
$k_{vi,1}$, $k_{vi,2}$	100	$R_{C,3}$	0.1 Ω	$R_{C,4}$	0.1 Ω
$v_{bus,1}$, $v_{bus,2}$	24 V	$k_{vp,3}$	0.65	$k_{vp,4}$	0.9
$L_{n,1}$	100 μH	$k_{vi,3}$	100	$k_{vi,4}$	200
$R_{Ln,1}$	0.05 Ω	$v_{o,3}$	15 V	$v_{o,4}$	12 V
$k_{vp,2}$	0.1	R_3	3 Ω		

1) Stability Analysis: Assume that all line admittances can be expressed as $Y_{1,2}(s) = 1/(L_{n,1}s + R_{Ln,1})$, $Y_{1,3}(s) = 1/(L_{n,2}s + R_{Ln,2})$, and $Y_{2,4}(s) = 1/(L_{n,3}s + R_{Ln,3})$. Based on (5)–(7) and Fig. 11(a), there are

$$\boldsymbol{Y}_{\text{in}}(s) = \text{diag}\,[1,\ 1,\ -Y_3(s),\ -Y_4(s)] \tag{29}$$

$$\boldsymbol{Z}_o(s) = \text{diag}\,[Z_1(s),\ Z_2(s),\ -1,\ -1] \tag{30}$$

$$\boldsymbol{Y}_{\text{net}}(s) = \begin{bmatrix} Y_{1,2}(s)+Y_{1,3}(s) & -Y_{1,2}(s) & -Y_{1,3}(s) & 0 \\ -Y_{1,2}(s) & Y_{1,2}(s)+Y_{2,4}(s) & 0 & -Y_{2,4}(s) \\ -Y_{1,3}(s) & 0 & Y_{1,3}(s) & 0 \\ 0 & -Y_{2,4}(s) & 0 & Y_{2,4}(s) \end{bmatrix}. \tag{31}$$

By substituting (29)–(31) into (3), the pole-zero plots of the determinant det[$\boldsymbol{T}_m(s)$] in two cases can be drawn, as displayed in Fig. 12. When the system operates in case III, det[$\boldsymbol{T}_m(s)$] has no RHP zeros, whereas in case IV, det[$\boldsymbol{T}_m(s)$] contains a pair of RHP zeros at 332 Hz. According to the proposed stability

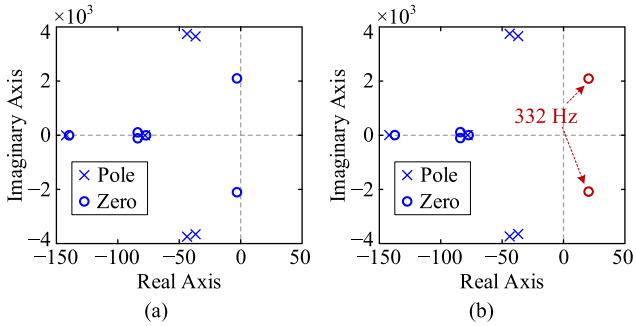

Fig. 12. Pole-zero plots of det[$\boldsymbol{T}_m(s)$] in two cases. (a) case III. (b) case IV.

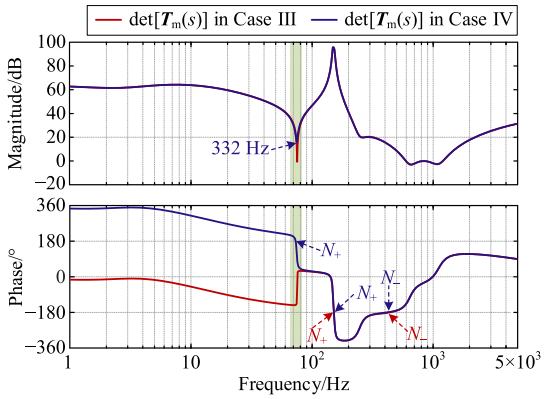

Fig. 13. Bode plots of det[$\boldsymbol{T}_m(s)$] in two cases.

analysis method, it can be inferred that the system is stable in case III, but unstable in case IV with the oscillation frequency being approximately 332 Hz.

Fig. 13 shows the Bode plots of det[$\boldsymbol{T}_m(s)$]. It can be found that in case III, there is N_+–N_- = 1–1 = 0, while in case IV, there is N_+–N_- = 2–1 = 1. According to the analysis in Section II-B, the Nyquist contour of det[$\boldsymbol{T}_m(s)$] does not encircle the origin in case III, but it encircles the origin clockwise twice in case IV. Therefore, the conclusion of system stability is consistent with the analysis results based on pole-zero plots mentioned above.

2) Instability Participation Analysis: In Case IV, four eigenvalues of $\boldsymbol{T}_m(s)$ at 332 Hz are calculated as $\lambda_1 = 31.6451 + j8.5963$, $\lambda_2 = 8.5433 + j4.7661$, $\lambda_3 = 0.0091$–$j0.0029$, and $\lambda_4 = -0.2788 + j2.0754$. Therefore, λ_3 is the critical eigenvalue because its amplitude is clearly the smallest. Subsequently, the participation factors associated with λ_3, i.e., $p_{3,1}$, $p_{3,2}$, $p_{3,3}$, and $p_{3,4}$, are calculated, and their magnitudes are plotted in Fig. 14. It is observed that around the predicted oscillation frequency, the participation factor of the dc bus node n_4 is more significant than the others, indicating that #4 converter has the highest instability participation in case IV. Note that unlike Section IV-A, the participation level of #3 converter cannot be ignored as its magnitude is significantly greater than those of # 1 and #2 converters. Therefore, the system stability in case IV is primarily sensitive to #4 converter, with secondary sensitivity to #3 converter.

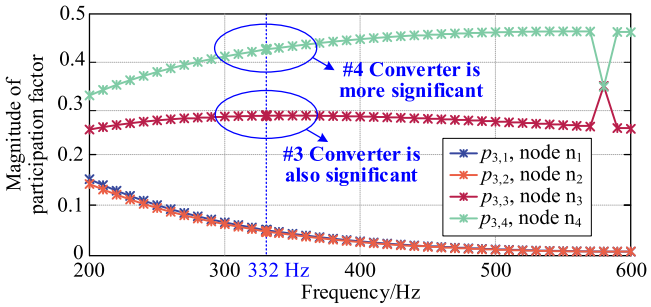

Fig. 14. Participation analysis of case IV.

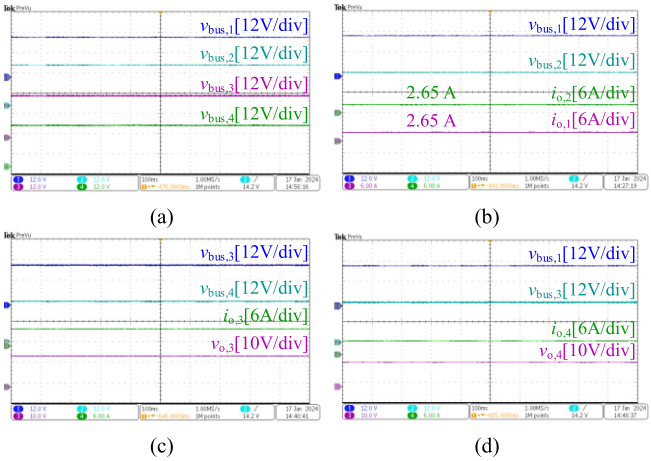

Fig. 15. Experimental waveforms in Case III. (a) $v_{\text{bus},1}$, $v_{\text{bus},2}$, $v_{\text{bus},3}$, and $v_{\text{bus},4}$. (b) $v_{\text{bus},1}$, $v_{\text{bus},2}$, $i_{o,1}$, and $i_{o,2}$. (c) $v_{\text{bus},3}$, $v_{\text{bus},4}$, $i_{o,3}$, and $v_{o,3}$. (d) $v_{\text{bus},1}$, $v_{\text{bus},3}$, $i_{o,4}$, and $v_{o,4}$.

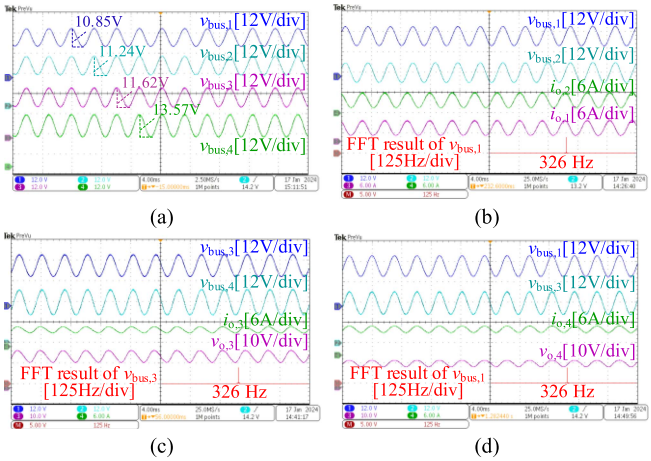

Fig. 16. Experimental waveforms in case IV. (a) $v_{\text{bus},1}$, $v_{\text{bus},2}$, $v_{\text{bus},3}$, and $v_{\text{bus},4}$. (b) $v_{\text{bus},1}$, $v_{\text{bus},2}$, $i_{o,1}$, and $i_{o,2}$. (c) $v_{\text{bus},3}$, $v_{\text{bus},4}$, $i_{o,3}$, and $v_{o,3}$. (d) $v_{\text{bus},1}$, $v_{\text{bus},3}$, $i_{o,4}$, and $v_{o,4}$.

3) Experiment Validations: Experimental results for the system in cases III and IV are presented in Figs. 15 and 16, respectively. Fig. 17 shows the dynamic experimental waveforms from case III to case IV. It can be seen that in case III, all voltage and current waveforms are stable, and the ratio of the output currents of #1 and #2 converters is in accordance with the coefficient

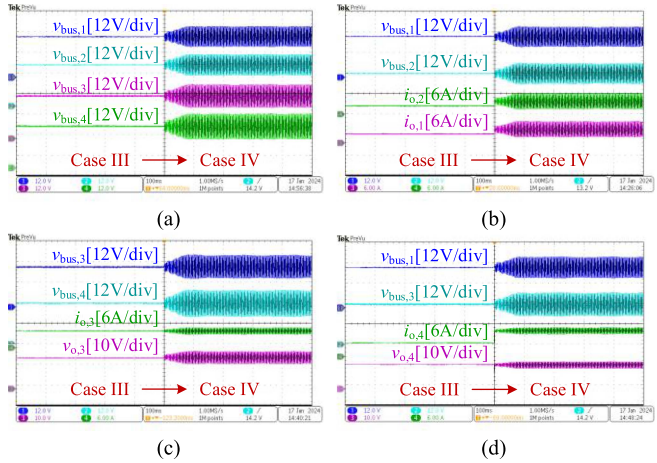

Fig. 17. Dynamic experimental waveforms from case III to case IV. (a) $v_{\text{bus},1}$, $v_{\text{bus},2}$, $v_{\text{bus},3}$, and $v_{\text{bus},4}$. (b) $v_{\text{bus},1}$, $v_{\text{bus},2}$, $i_{o,1}$, and $i_{o,2}$. (c) $v_{\text{bus},3}$, $v_{\text{bus},4}$, $i_{o,3}$, and $v_{o,3}$. (d) $v_{\text{bus},1}$, $v_{\text{bus},3}$, $i_{o,4}$, and $v_{o,4}$.

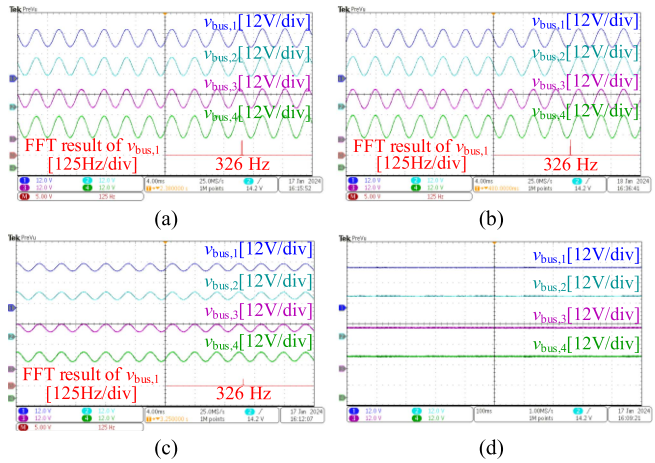

Fig. 18. Experimental voltage waveforms when the voltage-loop proportional coefficients change in case IV. (a) $k_{vp,1} = 0.1$. (b) $k_{vp,2} = 0.077$. (c) $k_{vp,3} = 0.5$. (d) $k_{vp,4} = 0.69$.

ratio of droop control, indicating that the entire system operates stably. In contrast, in case IV, the system is obviously unstable, with each node voltage containing significant ac components. FFT analysis of $v_{\text{bus},1}$ and $v_{\text{bus},3}$ reveals an oscillation frequency of approximately 326 Hz, which is also basically consistent with the aforementioned analysis results. Therefore, the experimental results of the two cases demonstrate the correctness of the proposed stability criterion.

To further validate the aforementioned conclusions on system instability participation analysis, based on the parameters in case IV, the voltage-loop proportional coefficients of four converters, i.e., $k_{vp,1}$, $k_{vp,2}$, $k_{vp,3}$, and $k_{vp,4}$, are reduced by 23%. In other words, these proportional coefficients are reduced to 0.1, 0.077, 0.5, and 0.69, respectively. The steady-state and dynamic experimental waveforms are shown in Figs. 18 and 19, respectively. Compared with Fig. 16, it can be found that: the system remains unstable when $k_{vp,1}$ and $k_{vp,2}$ decrease, and the change in oscillation amplitude is almost indistinguishable;

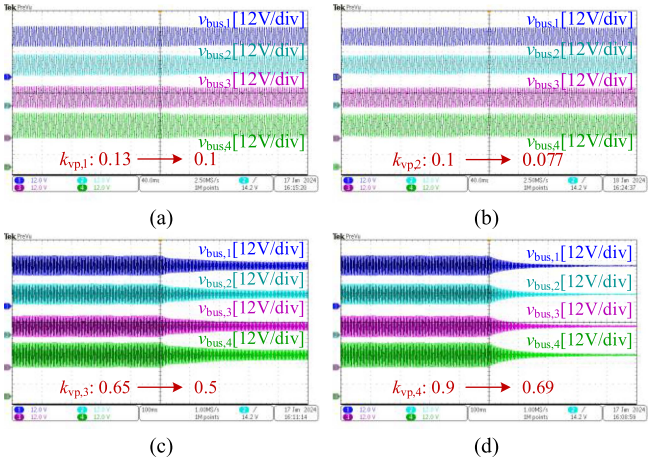

Fig. 19. Dynamic experimental waveforms when the voltage-loop proportional coefficients change in case IV. (a) $k_{vp,1}$ changes from 0.13 to 0.1. (b) $k_{vp,2}$ changes from 0.1 to 0.077. (c) $k_{vp,3}$ changes from 0.65 to 0.5. (d) $k_{vp,4}$ changes from 0.9 to 0.69.

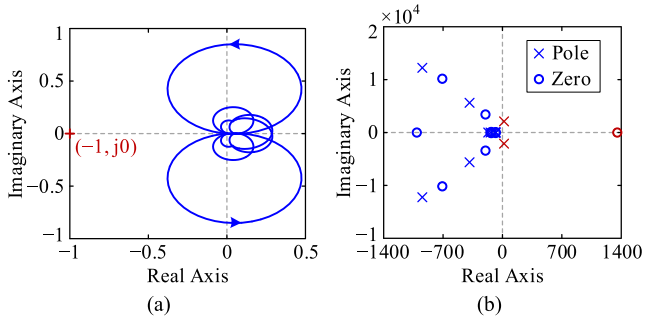

Fig. 20. Nyquist contour and zero-pole plots of impedance ratio in case IV (a) Nyquist contour. (b) Zero-pole plots.

when $k_{vp,3}$ decreases, the system is still unstable, but the oscillation amplitude is significantly reduced; and after $k_{vp,4}$ is reduced by 23%, the system becomes stable. Therefore, #4 converter is the critical instability source in case IV, and #3 converter also has a certain influence on the system stability, which is consistent with the aforementioned conclusion. In summary, the experiment results verify the proposed instability participation analysis method.

V. Discussion

A. Comparison Between Several Existing Stability Analysis Methods and the Proposed Stability Criterion

Several classical or similar stability analysis methods and the proposed stability criterion are compared as follows.

1) Comparison with Traditional Impedance Ratio Criterion: The traditional impedance ratio criterion originated from the Middlebrook criterion [11]. The Middlebrook criterion is just a sufficient condition for system stability, which is simple but conservative [10]. Subsequently, Zhang et al. [12] and Wang et al. [27] extended this criterion to the multiconverter parallel systems. By allocating all GVSs and all GCSs to two different subsystems, the impedance ratio is defined as the ratio of the equivalent impedances of two subsystems. However, for the dc microgrid shown in Fig. 1, we cannot find a specific node that can allocates all GVSs to one subsystem and all GCSs to the other one. In other words, the traditional impedance ratio criterion cannot be directly used in this article.

2) Comparison with Extended Impedance Ratio Criterion: Recently, several studies have indicated and demonstrated that the traditional impedance ratio criterion can be extended and applicable to the arbitrary divided subsystems [17], [29], [30], [31]. However, the extended impedance ratio may contain some RHP poles [17], [29], [31]. For example, if the 24 V 180 W dc microgrid is divided into two subsystems at node n_3. The Nyquist contour and zero-pole plots of impedance ratio in case IV are given in Fig. 20. It can be seen that although the Nyquist contour of impedance ratio dose not encircle the point (–1, *j*0), the dc microgrid is unstable due to the impedance ratio having two RHP poles.

By contrast, the proposed stability criterion does not contain any RHP pole, which is explicitly proven, thus, it requires fewer analysis steps. Meanwhile, the proposed stability criterion only needs to analyze phase, which is simpler and straightforward.

3) Comparison with Other Stability Analysis Methods: In Section I, several stability analysis methods for the dc systems with line network are discussed. Compared with these methods, the proposed stability criterion is not limited to a specific number of nodes, bypassing the RHP pole issue, with simplified impedance aggregation calculation and enhanced applicability to dc microgrids with unknown parameters.

To sum up, the proposed stability criterion has several obvious advantages compared to the existing methods.

B. Influence of Line Impedance

In this article, the line impedance affects the system modeling, stability analysis and results of dc microgrids, and the detailed reasons are as follows.

1) Impact on System Modeling and Stability Analysis: For the dc microgrid without considering the line impedance, the small-signal voltage equation is represented as a multi-input single-output transfer function model, and the impedance ratio used for stability analysis is a scalar transfer function [17]. However, for the dc microgrid with line impedance, the node voltage vector, i.e., (1) is a multi-input multioutput transfer function matrix model, and $\boldsymbol{T}_m(s)$ is a transfer function matrix. In the aforementioned analysis, the scalar determinant adj[$\boldsymbol{T}_m(s)$] is adopted to assess system stability. Therefore, the line impedance leads to completely different system modeling and stability analysis methods.

2) Impact on System Stability: The line impedance will also affect the system stability results, which has been analyzed and validated in [9]. In this article, we remove all line impedances of the 24 V 180 W dc microgrid. The stability analysis and experimental results of cases III and IV are shown in Figs. 21

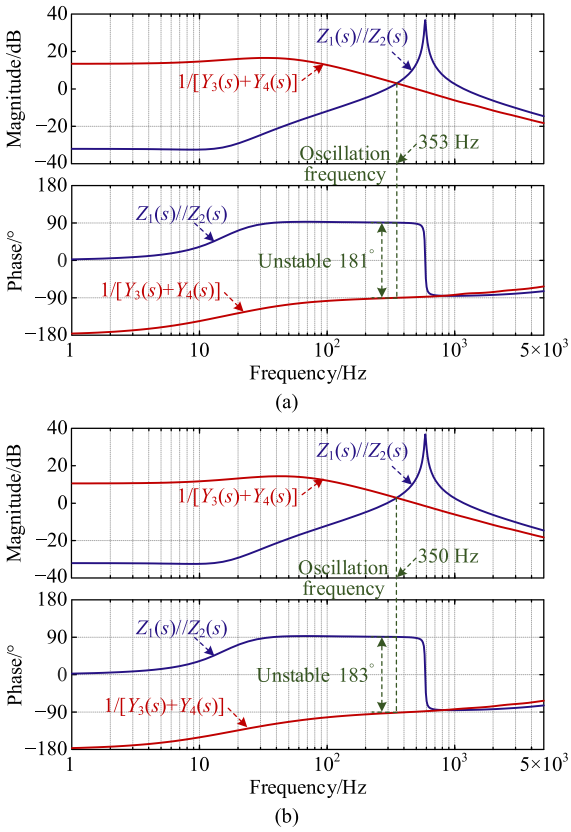

Fig. 21. Stability analysis of the 24 V 180 W dc Microgrid without line impedance. (a) case III. (b) case IV.

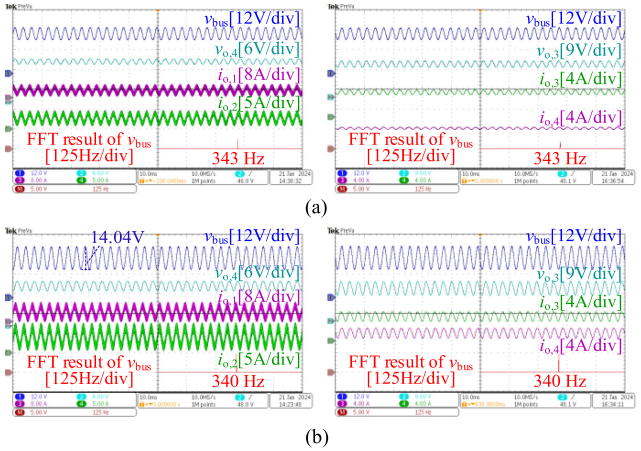

Fig. 22. Experimental waveforms of the 24 V 180 W dc Microgrid without line impedance. (a) case III. (b) case IV.

and 22, respectively. It can be seen that the line impedance significantly affects the system stability results, instability frequency and oscillation amplitude.

VI. Conclusion

In order to effectively assess the small-signal stability of dc microgrid, this article proposes a system-level stability criterion based on the determinant of the constructed immittance matrix. On this basis, an instability participation analysis method is further presented to identify the critical converters that lead to the system instability. Finally, case studies, simulations and experiments validate the correctness of the proposed approaches and theoretical analysis. The main conclusions are as follows.

1) Since the constructed immittance matrix contains no RHP poles when all converters are individually stable, the stability of dc microgrid can be evaluated solely by the phase of the determinant of the immittance matrix. Specifically, if the net number of times that the phase trajectory crosses the $\pm 180°$ line is zero, the system is stable, otherwise it is unstable.
2) The proposed frequency-domain instability participation analysis approach is based on the eigenvalues of the immittance matrix, which is completely different from existing methods based on the return-ratio matrix. At the system instability frequency, the smallest eigenvalue is identified as critical, and the participation factors are defined by the sensitivity of the critical eigenvalue to the equivalent immittance at each bus node.
3) There may be more than one converter significantly impacting system stability. When the parameters of the same type are changed in equal proportion, a larger participation factor indicates a greater influence on system stability.

References

[1] K. Karunanithi, S. Ramesh, S. P. Raja, and S. Saravanan, "Optimum sizing and modeling of stand-alone DC microgrid with hybrid energy storage system for domestic applications: Cost of energy, net present cost, and feasible configurations," *IEEE Syst., Man, Cybern. Mag.*, vol. 9, no. 2, pp. 18–24, Apr. 2023.
[2] B. He, W. Chen, H. Mu, D. Zhan, and C. Zhang, "Small-signal stability analysis and criterion of triple-stage cascaded DC system," *IEEE J. Emerg. Sel. Topics Power Electron.*, vol. 10, no. 2, pp. 2576–2586, Apr. 2022.
[3] H. Tu, H. Yu, and S. Lukic, "Dynamic nonlinear droop control (DNDC): A novel primary control method for DC microgrids," *IEEE Trans. Power Electron.*, vol. 39, no. 9, pp. 10934–10949, Sep. 2024.
[4] M. Nagpal, "Empowering energy evolution: The rise of microgrid autonomy," *IEEE Electrific. Mag.*, vol. 12, no. 2, pp. 6–11, Jun. 2024.
[5] X. Ge, X. Zhang, and H. Ma, "A semi-supervised learning framework based on EMD and SGAN for online stability monitoring of DC power electronic systems," *IEEE Trans. Ind. Electron.*, vol. 71, no. 10, pp. 12348–12357, Oct. 2024.
[6] H. Lin, H. S. H. Chung, R. Shen, and Y. Xiang, "Enhancing stability of DC cascaded systems with CPLs using MPC combined with NI and accounting for parameter uncertainties," *IEEE Trans. Power Electron.*, vol. 39, no. 5, pp. 5225–5238, May 2024.
[7] S. Jiang, Y. Zhu, and G. Konstantinou, "Settling-angle-based stability analysis for multiple current-controlled converters," *IEEE Trans. Power Electron.*, vol. 37, no. 11, pp. 12992–12997, Nov. 2022.
[8] S. Jiang and G. Konstantinou, "Impedance-based stability analysis: Nodal admittance or bus admittance?," *IEEE Trans. Power Syst.*, vol. 39, no. 1, pp. 2327–2340, Jan. 2024.
[9] B. He, W. Chen, X. Ruan, X. Zhang, Z. Zou, and W. Cao, "A generic small-signal stability criterion of DC distribution power system: Bus node impedance criterion (BNIC)," *IEEE Trans. Power Electron.*, vol. 37, no. 5, pp. 6116–6131, May 2022.
[10] A. Riccobono and E. Santi, "Comprehensive review of stability criteria for DC power distribution systems," *IEEE Trans. Ind. Appl.*, vol. 50, no. 5, pp. 3525–3535, Sep./Oct. 2014.
[11] R. D. Middlebrook, "Input filter considerations in design and application of switching regulators," in *Proc. IEEE Ind. Appl. Soc. Annu. Meet.*, 1976, pp. 366–382.
[12] X. Zhang, X. Ruan, and C. K. Tse, "Impedance-based local stability criterion for DC distributed power systems," *IEEE Trans. Circuits Syst. I, Reg. Papers*, vol. 62, no. 3, pp. 916–925, Mar. 2015.

[13] F. Liu, J. Liu, H. Zhang, and D. Xue, "Stability issues of Z + Z type cascade system in hybrid energy storage system (HESS)," *IEEE Trans. Power Electron.*, vol. 29, no. 11, pp. 5846–5859, Nov. 2014.
[14] F. Liu, J. Liu, B. Zhang, H. Zhang, and S. U. Hasan, "General impedance/admittance stability criterion for cascade system," in *Proc. IEEE ECCE Asia Downunder (ECCE Asia)*, Jun. 2013, pp. 422–428.
[15] W. Cao, K. Liu, S. Wang, H. Kang, D. Fan, and J. Zhao, "Harmonic stability analysis for multi-parallel inverter-based grid-connected renewable power system using global admittance," *Energies*, vol. 12, no. 14, Jul. 2019, Art. no. 2687.
[16] B. He, W. Chen, X. Li, L. Shu, Z. Zou, and F. Liu, "Unified frequency-domain small-signal stability analysis for interconnected converter systems," *IEEE J. Emerg. Sel. Topics Power Electron.*, vol. 11, no. 1, pp. 532–544, Feb. 2023.
[17] B. He, W. Chen, X. Li, L. Shu, J. Chen, and Y. Chen, "Impedance-based stability assessment methods for multi-paralleled converter systems," *CSEE J. Power Energy Syst.*, early access, doi: 10.17775/CSEEJPES. 2022.07320.
[18] Y. Zhang, X. Qu, G. Wang, J. Mei, H. H. C. Iu, and T. Fernando, "A combined bus port impedance based stability criterion for DC distribution power systems," *IEEE Trans. Smart Grid*, vol. 15, no. 5, pp. 4364–4376, Sep. 2024, doi: 10.1109/TSG. 2024.3382339.
[19] H. Hu, X. Wang, Y. Peng, Y. Xia, M. Yu, and W. Wei, "Stability analysis and stability enhancement based on virtual harmonic resistance for meshed DC distributed power systems with constant power loads," *Energies*, vol. 10, no. 1, Jan. 2017, Art. no. 69.
[20] J. Li, Y. Chen, J. Chen, X. Pei, H. Wu, and P. Chen, "Impedance-based stability analysis of DC distribution systems with complex network," in *Proc. IEEE 7th Int. Elect. Energy Conf.*, 2024, pp. 1715–1719.
[21] G. C. Verghese, I. J. Perez-arriaga, and F. C. Schweppe, "Selective modal analysis with applications to electric power systems, Part II: The dynamic stability problem," *IEEE Trans. Power Appl. Syst.*, vol. PAS-101, no. 9, pp. 3126–3134, Sep. 1982.
[22] Y. Li et al., "Stability analysis and location optimization method for multiconverter power systems based on nodal admittance matrix," *IEEE J. Emerg. Sel. Topics Power Electron.*, vol. 9, no. 1, pp. 529–538, Feb. 2021.
[23] Y. Liao, X. Wang, and X. Wang, "Frequency-domain participation analysis for electronic power systems," *IEEE Trans. Power Electron.*, vol. 37, no. 3, pp. 2531–2537, Mar. 2022.
[24] Y. Zhu, Y. Gu, Y. Li, and T. Green, "Participation analysis in impedance models: The grey-box approach for power system stability," *IEEE Trans. Power Syst.*, vol. 37, no. 1, pp. 343–353, Jan. 2022.
[25] Y. Liao, H. Wu, X. Wang, M. Ndreko, R. Dimitrovski, and W. Winter, "Stability and sensitivity analysis of multi-vendor, multi-terminal HVDC systems," *IEEE Open J. Power Electron.*, vol. 4, pp. 52–66, Jan. 2023.
[26] X. Meng, Q. Zhang, Z. Liu, G. Hu, F. Liu, and G. Zhang, "Multiple vehicles and traction network interaction system stability analysis and oscillation responsibility identification," *IEEE Trans. Power Electron.*, vol. 39, no. 5, pp. 6148–6162, May 2024.
[27] X. Wang et al., "Decentralized impedance specifications for small-signal stability of DC distributed power systems," *IEEE J. Emerg. Sel. Topics Power Electron.*, vol. 5, no. 4, pp. 1578–1588, Dec. 2017.
[28] J. Li et al., "Impedance-based instability participation analysis for DC distribution systems," in *Proc. IEEE 7th Int. Conf. Energy Elect. Power Eng.*, Apr. 2024, pp. 1074–1078.
[29] Y. Liao and X. Wang, "Impedance-based stability analysis for interconnected converter systems with open-loop RHP poles," *IEEE Trans. Power Electron.*, vol. 35, no. 4, pp. 4388–4397, Apr. 2020.
[30] H. Mu et al., "Impedance-based stability analysis methods for DC distribution power system with multivoltage levels," *IEEE Trans. Power Electron.*, vol. 36, no. 8, pp. 9193–9208, Aug. 2021.
[31] M. Leng, G. Zhou, H. Li, G. Xu, F. Blaabjerg, and T. Dragičević, "Impedance-based stability evaluation for multibus DC microgrid without constraints on subsystems," *IEEE Trans. Power Electron.*, vol. 37, no. 1, pp. 932–943, Jan. 2022.

Bangbang He (Member, IEEE) received the B.S. and M.S. degrees in electrical engineering from China University of Mining and Technology-Beijing, Beijing, China, in 2017 and 2020, respectively, and the Ph.D. degree in electrical engineering from Southeast University, Nanjing, China, in 2024.

He is currently a Lecturer with the School of Electrical and Electronic Engineering, North China Electric Power University. His research interests include stability analysis and design of dc distribution systems, HVDC grids, and energy saving of railway traction power systems.

Wu Chen (Senior Member, IEEE) received the B.S., M.S., and Ph.D. degrees from the Nanjing University of Aeronautics and Astronautics (NUAA), Nanjing, China, in 2003, 2006, and 2009, respectively, all in electrical engineering. From 2009 to 2010, he was a Senior Research Assistant with the Department of Electronic Engineering, City University of Hong Kong, Hong Kong. In 2010 and 2011, he was a Postdoctoral Researcher with Future Renewable Electric Energy Delivery and Management engineering research center, North Carolina State University, Raleigh, NC, USA. Since 2011, he has been an Associate Research Fellow with the School of Electrical Engineering, Southeast University, Nanjing, China, where he has been a Professor since 2016. He is the Director of the Center for Advanced Power-Conversion Technology and Equipment, including three professors, five associate professors and nearly 100 postgraduate students. He is also the Deputy Director of the Academic Committee of the Department of Electronic Engineering. He has authored or coauthored three books and more than 120 technical articles published in journals and conference papers. His research areas include soft-switching dc–dc converters, MMC, high power converters for ac/dc hybrid distribution network, and ac/dc system stability analysis.

Dr. Chen is currently an Associate Editor for IEEE TRANSACTIONS ON INDUSTRIAL ELECTRONICS, *Journal of Power Electronics*, *CPSS Transactions on Power Electronics and Applications*, *Journal of Power Supply*, and *High Voltage Engineering*.

Jianzhong Xu (Senior Member, IEEE) was born in Shanxi, China. He received the Ph.D. in electrical engineering from North China Electric Power University (NCEPU), Beijing, China, in 2014.

He is currently a Professor with the State Key Laboratory of Alternate Electrical Power System with Renewable Energy Resources, NCEPU. His research interests include electromagnetic transient equivalent modeling, simulation, and analysis of HVdc grid.

Han Mu (Student Member, IEEE) received the B.S. degree in automation from Northeast Electric Power University, Jilin City, China, in 2018, and the M.S. degree in electrical engineering from Southeast University, Nanjing, China, in 2021. She is currently working toward the Ph.D. degree in electrical engineering with the Eindhoven University of Technology, Eindhoven, The Netherlands.

Her research interests include system-level layout design, modeling, and stability analysis for large-scale power electronics-based renewable energy systems.

Chengyong Zhao (Senior Member, IEEE) was born in Zhejiang, China. He received the B.S., M.S. and Ph.D. degrees in power system and its automation from North China Electric Power University, Beijing, China, in 1988, 1993 and 2001, respectively.

He was a Visiting Professor with the University of Manitoba, from January 2013 to April 2013 and September 2016 to October 2016. Currently, He is currently a Professor with the School of Electrical and Electronic Engineering, NCEPU. His research interests include HVDC system and dc grid.